Towards time resolved tip-enhanced Raman spectroscopy: TERS with chopped laser pulses

Ana M[a]. Gómez–Marín[a,b*], Katrin F. Domke[a,*]

[a] University of Duisburg-Essen, Faculty of Chemistry, Physical Chemistry II, Essen, Germany.

[b] Department of Chemistry, Division of Fundamental Sciences (IEF), Technological Institute of Aeronautics (ITA), São José dos Campos CEP: 12228-900, SP, Brazil.

* Corresponding author. Tel.: +55 12 3947 6852. E-mail address: agomezma@ita.br (A.M. Gómez–Marín). E-mail address: katrin.domke@uni-due.de (K.F. Domke).

1. Experimental setup

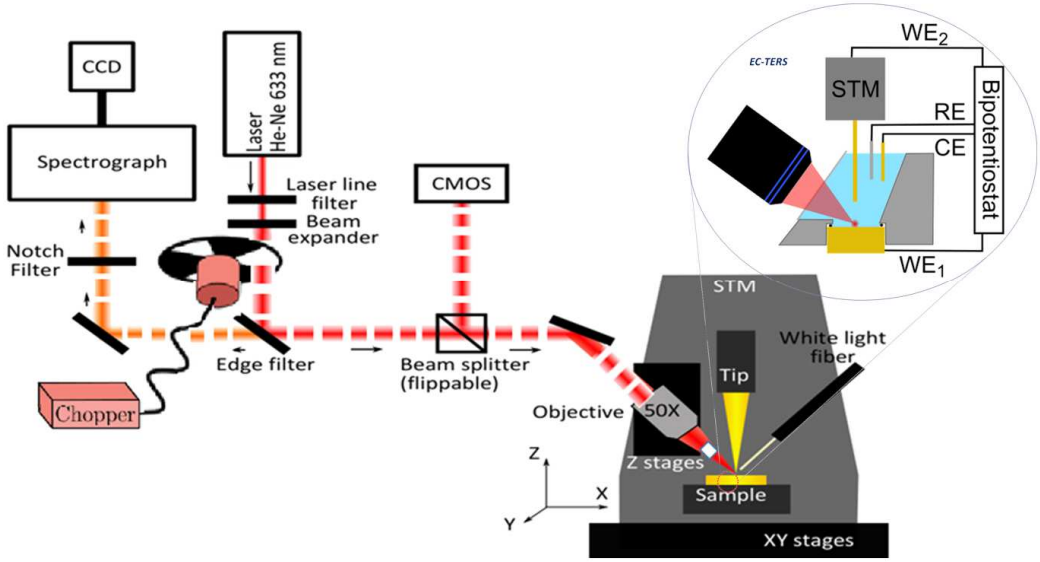

Figure S1. Schematics of the beam path of the TERS setup (adapted from reference 1).

2. Spectra fitting

For extracting peak's parameters of the TERS PhS/Au(111) signal, the background of raw spectra (Fig. S2A), after cosmic rays removal, was initially fitted with the ALS algorithm,[2,3,4] as implemented into the open-source Python library for Raman spectroscopic analysis, RamanSPy.[5] In this way TERS spectra were split into two parts: the TERS peaks and TERS background (Fig. S2B). Afterwards, each background - subtracted TERS spectrum (Fig. S2C) was divided by its own background spectrum, resulting in the Surface Plasmon Resonance (*spr*) - corrected TERS spectrum (Fig. S2D).

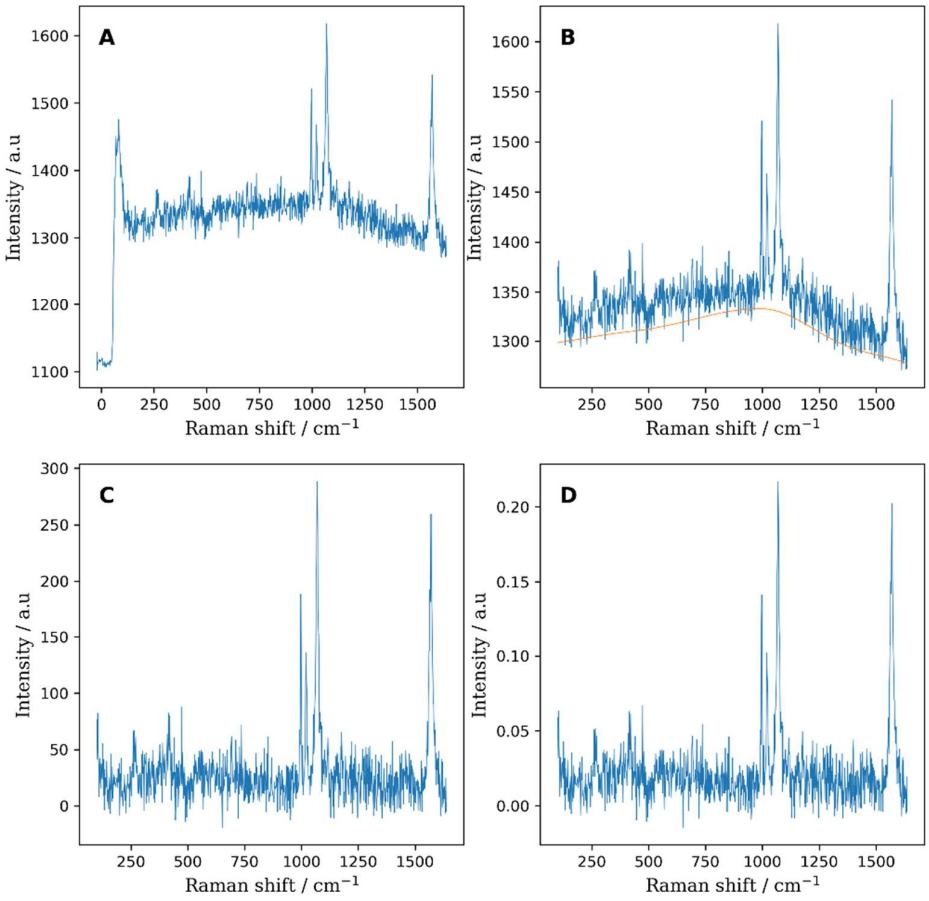

Figure S2. Preprocessing routine before mathematical fitting of TERS spectra. (A) Raw spectrum taken with P_{av} = 1.1 mW μm^{-2} and t_{aq} = 5 s under mechanically chopped laser pulses at 1000 Hz. (B) ALS fitted baseline. (C) TERS spectrum after background subtraction. (D). Normalized TERS spectrum by the TERS background.

Then, PhS peaks from both, background - subtracted TERS spectrum (Fig. S2C), and *spr*-corrected TERS spectrum (Fig. S2D) were fitted to Lorentzian curves by employing a Python library designed for non-linear least-squares minimization and curve fitting, LMFIT. For this process, the spectrum was first normalized to the maximum intensity value, and then cropped around wavenumber values associated with the peak spectral region of interest. Four peaks were fitted, three within the spectral region from 950 to 1150 cm^{-1}, corresponding to the characteristic ring stretches of PhS (Fig. S3A), and one within the spectral region around 1570 cm^{-1} (Fig. S3B), assignment to the C = C aromatic stretching.[1,6,6] Both, background - subtracted and *spr* - corrected TERS gave similar results and, thus, only data from spr – corrected spectra were reported in the manuscript.

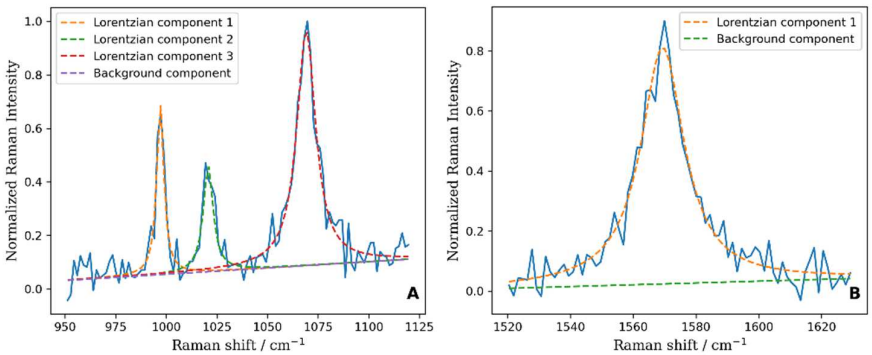

Figure S3. Mathematical fitting of Normalized *spr* - corrected PhS/Au(111) TERS spectrum in Fig. S2D. (A) Spectral region of the triplet of peaks, 997, 1021, and 1069 cm^{-1} (solid line). (B) 1569 cm^{-1} peak. Fitted Lorentzian peaks, and baselines are also included (dashed lines).

3. Band positions and assignments

The assignment of PhS/Au(111) Raman bands was performed based on reported data for similar systems. Table S1 resumes an abbreviated list of theoretical Raman band assignments for liquid PhS and adsorbed PhS/Au systems. Experimental data for liquid PhS is also given. A more complete assignment of the PhS Raman vibrational bands can be found elsewhere.[8,9]

Table S1. Theoretical Raman shifts (cm^{-1}) and vibrational mode assignments reported for liquid PhS, and PhS-Au SAMs.

Vibrational mode	Theoretical data from Ref. 8 (PhS/ PhS-Au)	Theoretical data from Ref. 9 (PhS/ PhS-Au)	Exp. from neat PhSH[8,9]
C–S stretching (ν_{CS})[a] and ring in-plane deformation, r-i-d, (δ_{CCC})[a], 7a(a_1)[b]	404/408	393/397 ($\nu_{CS} + \nu_{AuS}$)	412
Ring out-of-plane deformation, r-o-d, (γ_{CCC})[a], 4(b_1)[b]	693	672/668 (ω_{CH} + r-o-d)	689
r-i-d and ν_{CS}[a], 6a(a_1)[b]	696/702	678/674 (δ_{CCC} + r-i-d)	697
r-o-d and C–H out-of-plane bending (γ_{CH})[a], 5(b_1)[b]	989/999	942/950 (γ_{CH})	991
r-i-d and ν_{CC}[a], 12(a_1)[b]	990	976/975	1000
r-i-d and ν_{CC}[a], 18a(a_1)[b]	1018/1017	1006/1002 ($\nu_{CC} + \delta_{CH}$)	1024
C–C asymmetric stretching (ν_{CC}[a] as), 18b(b_2)[b]	1076	1064/1059 ($\nu_{CC} + \delta_{CH}$)	1070
ν_{CC}[a] and ν_{CS}[a], 1(a_1)[b]	1086/1064	1070/1049 ($\nu_{CS} + \delta_{CH} + \nu_{CC}$)	1092
ν_{CC}[a], 8a(a_1)[b]	1580/1569	1570/1559	1581

[a] γ, δ, and ν indicate out-of-plane bending, in-plane bending and stretching mode, respectively.

[b] Notation and normal modes for mono-substituted benzene rings as reported in 10.

4. Analysis of TERS temporal signal stability

Figure S4 resumes the time evolution of the *spr*-corrected TERS spectra, normalized to t = 0 s, under both laser excitations within a 10 min time window. The analysis of these data by following the variation of the peak intensity with time with a chopped cw beam at 1000 Hz is shown in Figure S5. Data were fitted to a first-order kinetics ($e^{-t/\tau}$) functional form, Figs. S5A, C, E and G, and to a functional form of the type ($t^{-1/2}$) to evaluate the suitability of a surface diffusion mechanism to describe the mechanism of TERS signal decay, Figs. S5B, D, F and H, for ~999, ~1021, ~1071, and ~1575 cm^{-1} peaks, respectively. Analogous data for TERS spectra with cw (A, C, E, G), and chopped pulsed light at 2000 Hz (B, D, F, H) fitted to a surface diffusion mechanism is given in Figure S6, in addition to the first-order kinetics ($e^{-t/\tau}$) functional form already discussed in Fig 2 in the text.

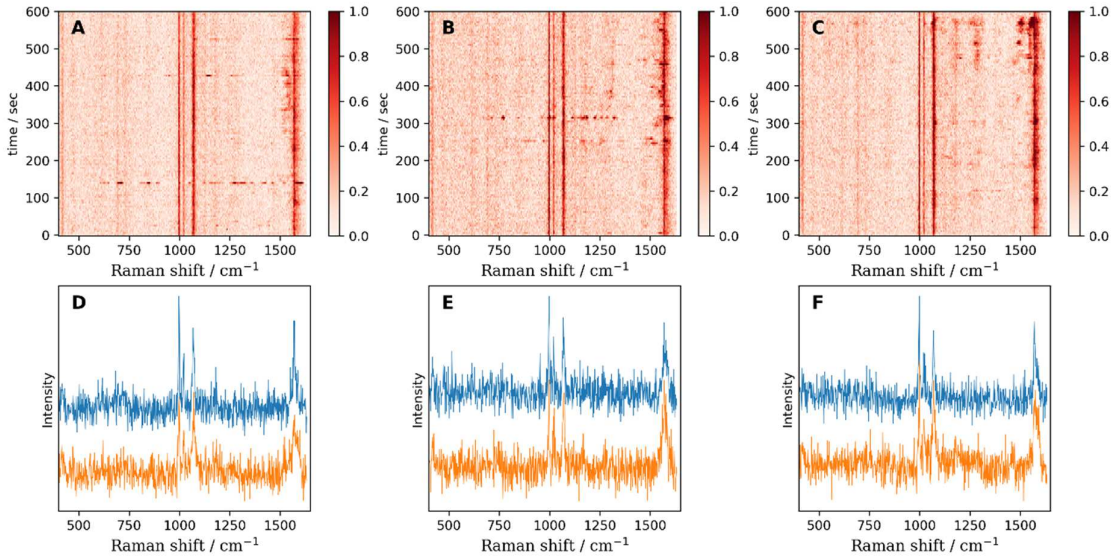

Figure S4. Time series waterfall plots, and initial (upper) and final (lower) TERS spectra of PhS/Au(111) at P_{av} = 1.1 mW μm^{-2} and t_{aq} = 5 s under a cw (A, D), and mechanically chopped cw at 1000 Hz (B, E), and 2000 Hz (C, F). In A – C spectra are normalized by the Raman intensity at t = 0 s, while in D – F initial spectra are y-offset for clarity.

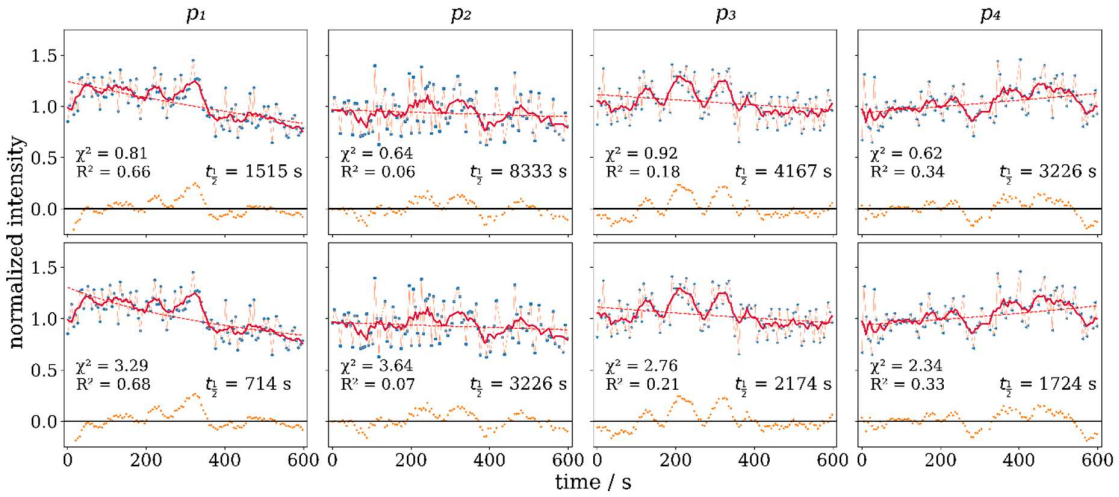

Figure S5. Time series of the intensities of p_1 to p_4 PhS/Au(111) TER peaks with a mechanically chopped cw at 1000 Hz excitations at P_{av} = 1.1 mW μm^{-2} shown in Fig. S4B. Data (blue dots) are normalized to the respective value at t = 0. For clarity, five-points weighted average curves are also given as solid red line. Dashed red lines are the exponential, $e^{-t/\tau}$, (top row), and inverse square root, $t^{-½}$, (bottom row) fits to the data. Fit residuals are plotted on y = 0 (yellow dots). The sum of the square of the residual of the fit (χ^2) and R^2 values together with the calculated signal half-life are noted for each case.

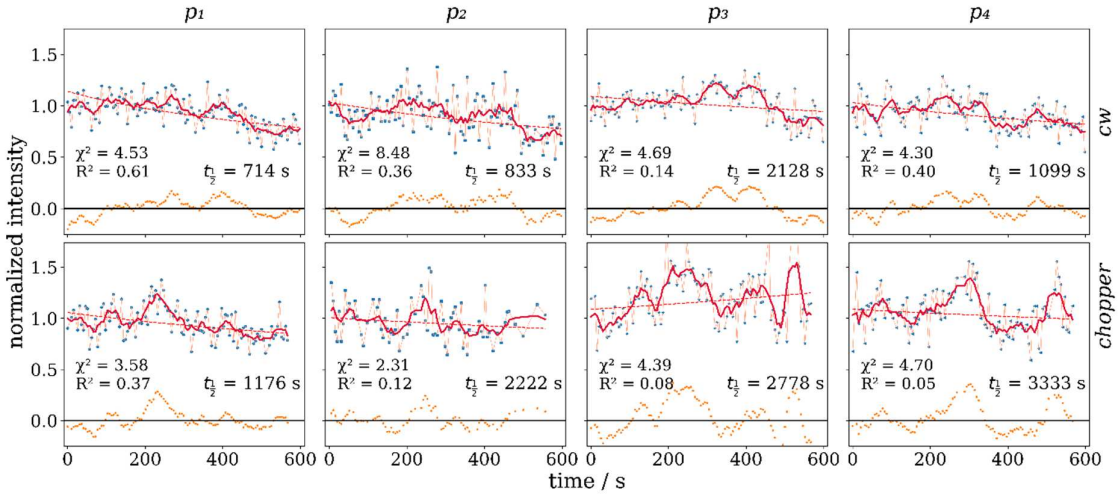

Figure S6. Time series of the intensities of p_1 to p_4 PhS/Au(111) TER peaks with cw (top row) and mechanically chopped cw at 2000 Hz (bottom row) excitations at P_{av} = 1.1 mW μm^{-2} shown in Figs. S4A and C, respectively. Dashed red lines are the inverse square root, $t^{-½}$, fits to the data. Other conditions are the same as in Fig. S5.

5. Dependence of the intensity of TERS signal on the power density

Figure S7 resumes the PhS/Au(111) TERS peak area of 999, 1021, 1071, and 1575 cm^{-1} as a function of P_{av} with a continuous wave (Figs. S7A, D, G, J), and mechanically chopped light pulses at 1000 (Figs. S7B, E, H, K), and 2000 Hz (Figs. S7C, F, I, L) excitations, respectively, at low P_{av}.

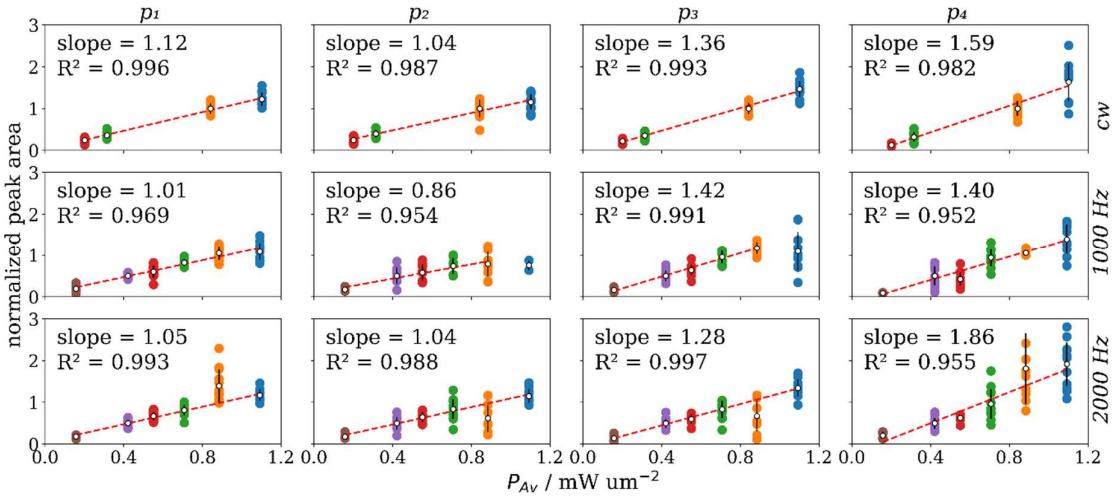

Figure S7. Dependence of TERS peak area on P_{av} for p_1 to p_4 with cw (top row), and mechanically chopped cw at 1000 Hz (middle row), and 2000 Hz (bottom row) excitations at low P_{av}. Areas are normalized to the area at 0.8 mW μm^{-2} (equivalent to the 0.5 in the figures under the chopped beam). Dashed lines are linear fits to the respective data. Fitted slopes and R^2 values are indicated.

5.1 Peak position, peak width and SNR

Figures S8, S9 and S10 show box charts for signal-to-noise ratios (SNR), changes in the spectral position relative to the average peak's Raman shift (spectral wandering), and peak widths from fitted TERS spectra for the selected four PhS Raman peaks discussed in the text as a function of the average laser power density, P_{av}. Data for 999 (A, B, C), 1021 (D, E, F), 1071 (G, H, I), and 1575 cm^{-1} (J, K, L) with a cw excitation are presented in figures A, D, G, and J, while with mechanically chopped laser pulses at 1000 Hz and 2000 Hz in figs. B, E, H, and K, and C, F, I, and L, respectively.

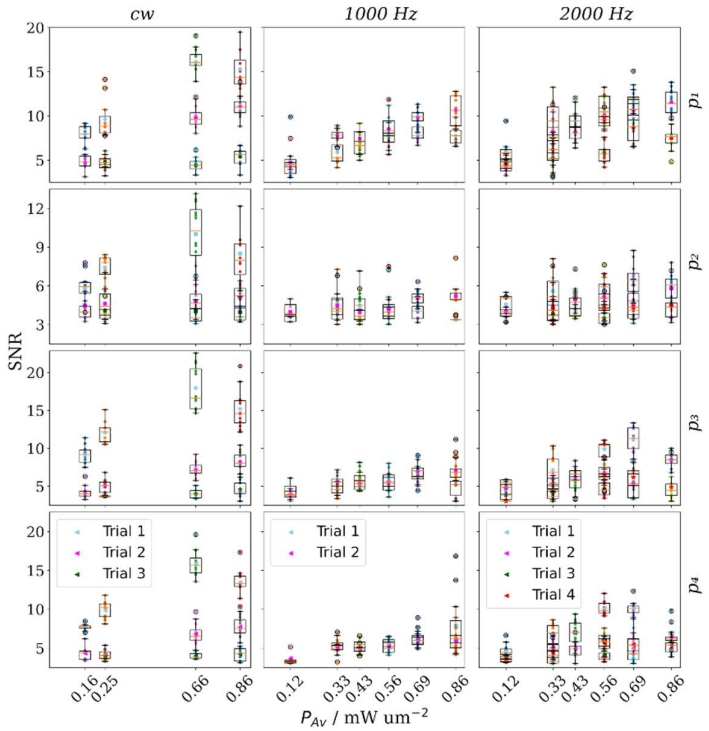

Figure S8. Box charts for the signal-to-noise ratio of fitted p_1 to p_4 PhS/Au(111) TER peaks at different P_{av}. The different symbols represent measurements on different samples. Conditions are the same as in Fig. S7.

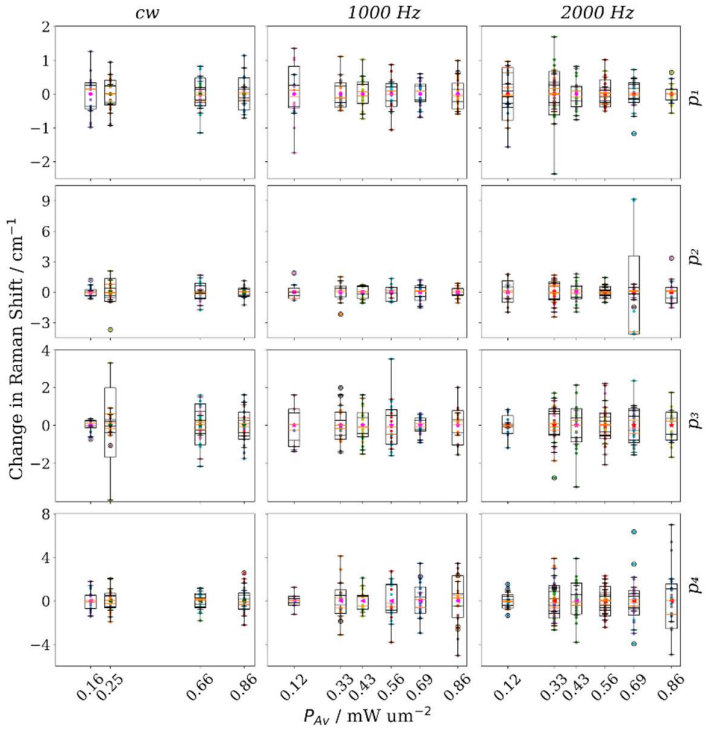

Figure S9. Box charts for the change in the Raman shift of fitted p_1 to p_4 PhS/Au(111) TER peaks at different P_{av}. Conditions are the same as in Fig. S8.

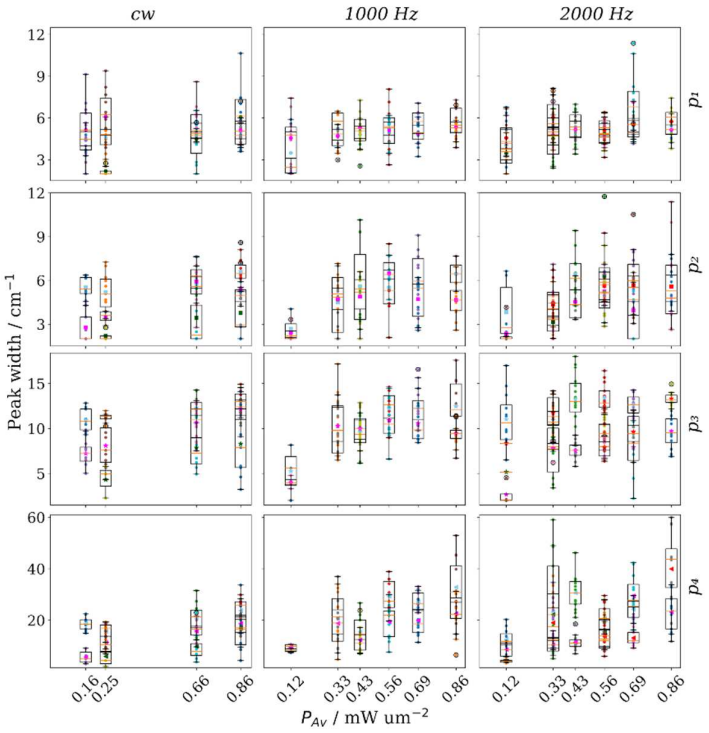

Figure S10. Box charts for the peak width of fitted p_1 to p_4 PhS/Au(111) TER peaks at different P_{av}. Conditions are the same as in Fig. S8.

References

1. N. Martín Sabanés, L. Driessen, K. F. Domke. A Versatile Side-Illumination Geometry for Tip-Enhanced Raman Spectroscopy at Solid/Liquid Interfaces. Anal. Chem 88 (2016) 7108-7114.
2. H. F. Boelens, P. H. Eilers. T. Hankemeier. Sign constraints improve the detection of differences between complex spectral data sets: LC-IR as an example. Anal. Chem. 77 (2005) 7998-8007.
3. P. H. C. Eilers, H. F. M. Boelens. Baseline correction with asymmetric least squares smoothing, Leiden University Medical Centre report 1 (2005) 24pp.
4. K. -Q. Lin, J. Yi, J. -H. Zhong, S. Hu, B. -J. Liu, J. -Y. Liu, C. Zong, Z. -C. Lei, X. Wang, J. Aizpurua, R. Esteban. B. Ren. Plasmonic photoluminescence for recovering native chemical information from surface-enhanced Raman scattering. Nature Commun. 8 (2017) 14891.

5. D. Georgiev, S. Vilms Pedersen, R. Xie, A. Fernandez-Galiana, M. M. Stevens, M. Barahona. RamanSPy: An open-source Python package for integrative Raman spectroscopy data analysis. Anal. Chem. 96 (2024) 8492-8500.
6. C. Blum, L. Opilik, J. M. Atkin, K. Braun, S. B. Kämmer, V. Kravtsov, N. Kumar, S. Lemeshko, J.-F. Li, K. Luszcz, T. Maleki, A. J. Meixner, S. Minne, M. B. Raschke, B. Ren, J. Rogalski, D. Roy, B. Stephanidis, X. Wang, D. Zhang, J.-H. Zhong, R. Zenobi. Tip-enhanced Raman spectroscopy – an interlaboratory reproducibility and comparison study. J. Raman Spectrosc. 45 (2014) 22-31.
7. N. Martín-Sabanés, A. Elizabeth, J. H. K. Pfisterer, K. F. Domke. The Effect of STM Parameters on Tip-Enhanced Raman Spectra. Faraday Discuss 205 (2017) 233–243.
8. S. Li, D. Wu, X. Xu, R. Gu. Theoretical and Experimental Studies on the Adsorption Behavior of Thiophenol on Gold Nanoparticles. J. Raman Spectrosc. 38 (2007) 1436−1443.
9. C. G. Tetsassi Feugmo, V. Liegeois. Analyzing the Vibrational Signatures of Thiophenol Adsorbed on Small Gold Clusters by DFT Calculations. ChemPhysChem 14 (2013) 1633-1645.
10. C. A. Szafranski, W. Tanner, P. E. Laibinis, R. L. Garrell. Surface-Enhanced Raman Spectroscopy of Aromatic Thiols and Disulfides on Gold Electrodes. Langmuir 14 (1998) 3570-3579.